Research Square

Preprints are preliminary reports that have not undergone peer review.
They should not be considered conclusive, used to inform clinical practice,
or referenced by the media as validated information.

Growth-vigour differentiation in whole-stem axial form and released growth strain of plantation Eucalyptus

kaixiang xu
Guangxi University
Jingzhen Huang
Guangxi University
Yunlin Fu
Guangxi University
Huaisi Zhai
Guangxi University
Penglian Wei
ztzxwpl@163.com

Guangxi University

Research Article

Keywords: Eucalyptus, growth vigour, whole-stem form, released growth strain, axial variation, xylem structure

Posted Date: November 12th, 2026

DOI: https://doi.org/10.21203/rs.3.rs-11441840/v1

License: This work is licensed under a Creative Commons Attribution 4.0 International License.
Read Full License

Additional Declarations: No competing interests reported.

Growth-vigour differentiation in whole-stem axial form and released growth strain of plantation *Eucalyptus*

Kaixiang Xu[1], Jingzhen Huang[1], Yunlin Fu[1], Huaisi Zhai[1], Penglian Wei[1],*

[1] Guangxi Colleges and Universities Key Laboratory for Cultivation and Utilization of Subtropical Forest Plantation, Guangxi Key Laboratory of Forest Ecology and Conservation, School of Forestry, Guangxi University, No. 100 Daxue East Road, Xixiangtang District, Nanning 530004, Guangxi, China

* Corresponding author: Penglian Wei (ORCID: 0000-0002-9028-1824); E-mail: ztzxwpl@163.com

Running title: Growth vigour, whole-stem form and released strain

Abstract

Background: Growth-vigour classes in even-aged plantations are usually distinguished by attained size, yet size alone does not show whether social differentiation extends to whole-stem construction and xylem mechanical state. We tested whether breast-height form represents the stem as a whole, whether axial geometry and released growth strain differ among vigour classes, and whether axial descriptors add information beyond tree size and local form.

Results: Twenty-four trees representing four growth-vigour classes in an 8-year-old plantation of *Eucalyptus urophylla* × *Eucalyptus grandis* were measured repeatedly along the stem, and released growth strain was measured in four cardinal directions at breast height. Breast-height form showed little agreement with the mean state at the other sampled heights (Lin's concordance correlation coefficients = 0.025-0.114). Cross sections became more regular upwards, while normalised major- and minor-diameter trajectories differed among vigour classes. Mean absolute released growth strain decreased from class A to D, whereas its within-tree standard deviation, range and coefficient of variation increased. In hierarchical models,

adjusted R^2 for mean absolute strain increased from 0.225 with tree size to 0.585 after breast-height form was added and to 0.890 after axial form was included; leave-one-tree-out Q^2 increased from -0.063 to 0.407 and 0.860. Axial form did not improve models of strain dispersion. In six purposively selected trees, higher strain tended to coincide with lower microfibril angle, higher cellulose crystallinity and variation in fibre-wall and relative FTIR traits.

Conclusions: Growth-vigour differentiation was expressed not only in attained size but also in whole-stem axial organisation and released-strain pattern. Repeated axial measurements captured biological variation that was poorly represented by a single breast-height section and added information specifically about mean strain magnitude rather than circumferential heterogeneity.

Keywords: Eucalyptus; growth vigour; whole-stem form; released growth strain; axial variation; xylem structure

Background

Even-aged plantations progressively differentiate into dominant and suppressed individuals as competition changes access to light, growing space, water and nutrients. Diameter at breast height (DBH), total height and height-to-diameter ratio describe attained size, but they do not reveal how growth has been distributed within the stem. Competition modifies plantation-tree allometry [6], growing space affects crown geometry [28], and past growth can leave a structural legacy in current development [24]. Growth vigour integrates crown position, crown exposure, relative height and dominance status and is therefore relevant to silvicultural assessment [10]. The central biological question is whether this social differentiation is expressed only in final size or also in the spatial construction and mechanical state of the stem.

Stem form records the cumulative outcome of radial growth, crown architecture, wind exposure, gravitational loading and developmental history [22]. Taper descriptors show how diameter is distributed along the bole [19], while information from log end faces and taper can reveal longitudinal departures in harvested stems [25]. A breast-height cross section characterises only one local position. Repeated cross sections additionally show how diameter attenuation, cross-sectional regularity and measured diameter orientations change from the stem base towards the crown. If growth-vigour classes differ in whole-stem allocation, those differences should be expressed more clearly in axial trajectories than in a single breast-height section.

Released growth strain provides a functional measure of the mechanical state generated during xylem maturation. Maturation stresses contribute to posture regulation and reaction-wood function [1], and their release after harvest is associated with splitting and distortion [15, 29]. In *Eucalyptus* plantations, released strain varies among provenances and developmental stages [3, 31]. Water availability [23] and tree-level growth conditions [18] provide further sources of variation. Mean absolute strain and circumferential dispersion need not respond in parallel: the former describes average released-strain magnitude, whereas the latter describes how unevenly that state is expressed around a tree. Growth-vigour differentiation may therefore involve both the level and the spatial heterogeneity of released strain.

The maturing xylem provides a possible structural context for these mechanical differences. Microfibril angle influences longitudinal cell-wall organisation and mechanical behaviour [4, 9], while cellulose crystallinity and fibre morphology describe additional dimensions of wood structure [2]. Reaction-wood anatomy and wall organisation vary among taxa and mechanical settings [14, 16], and cellulose microfibril orientation is regulated in a context-dependent manner during reaction-wood formation [30]. In the present study, these traits were available for only six

purposively selected trees. They were therefore examined as exploratory structural covariates, not as a population-level test of mechanism.

We studied 24 trees representing four growth-vigour classes in an 8-year-old plantation of *Eucalyptus urophylla* × *Eucalyptus grandis*. Three hypotheses were tested. H1: growth-vigour classes would overlap in local breast-height form but differ in size-corrected axial diameter trajectories. H2: mean absolute released growth strain would decline from dominant to suppressed trees, whereas circumferential heterogeneity would increase. H3: axial form would add information about mean absolute released growth strain beyond tree size and breast-height form. We first evaluated how well breast-height traits represented the mean state of the remaining sampled stem, then quantified axial geometry and released-strain patterns and finally tested their tree-level coordination. The six-tree xylem subset was retained as exploratory structural context.

Methods

Study site and sampling design

The study was conducted in a pure *Eucalyptus* plantation in the Guigang Afforestation Division of Liangfengjiang Forest Farm, Guangxi Zhuang Autonomous Region, China. The site has a subtropical humid monsoon climate, with a mean annual temperature of 18-22 °C, mean annual precipitation of approximately 1200 mm, an elevation of 70-100 m and gentle slopes of 3-5%. The soil was locally classified as lateritic red soil. Liangfengjiang Forest Farm is a state-owned forest farm directly administered by the Forestry Administration of Guangxi Zhuang Autonomous Region. Permission to conduct the study and collect plant material was granted by Liangfengjiang Forest Farm, which manages the study site. Sampling was conducted in accordance with relevant institutional and national guidelines and regulations.

The plantation was established in June 2017 and sampled in mid-July 2025. The 8-year-old *Eucalyptus urophylla* × *Eucalyptus grandis* DH32-26 trees were planted at 2 m × 3 m, corresponding to approximately 1667 trees ha^{-1}. Two 20 m × 20 m plots were established. All trees with DBH > 5 cm were measured for DBH, total height and height-to-diameter ratio (H/D, m cm^{-1}; Table 1).

The planted material was the cultivated, clonally propagated hybrid DH32-26 (*Eucalyptus urophylla* U16 [female] × *E. grandis* G46 [male]), bred by Guangxi Dongmen State-owned Forest Farm and registered as improved forest-tree clone Gui S-SC-EUG-001-2004. Clone identity was verified from the plantation establishment records held by Liangfengjiang Forest Farm rather than inferred from a wild-collected specimen. DH32-26 is registered commercial planting material, and no wild plants were collected or described in this study; therefore, the requirement for a wild-plant voucher specimen was not applicable.

Table 1. Stand characteristics of the experimental plantation.

Plot	Mean DBH (cm)	Mean height (m)	H/D (m cm^{-1})	Canopy closure	Elevation (m)	Slope (°)	Soil type	n
1	18.17 ± 2.92	22.86 ± 2.37	1.28 ± 0.16	0.9	80	3	Lateritic red soil	79
2	17.27 ± 2.70	23.68 ± 2.37	1.39 ± 0.14	0.8	84	5	Lateritic red soil	65

Values are means ± standard deviations; n is the number of trees with DBH > 5 cm.

Following Kraft classification, trees were assigned to four growth-vigour classes from crown position, crown exposure, relative height and dominance status: A, dominant; B, subdominant; C, intermediate; and D, suppressed. Class assignment was made consistently by the same observer from field crown status and relative tree position; the operational field rubric is provided in Additional file 1. Six trees were sampled per class, with three trees from each plot. Six trees were purposively selected to span classes A-D and the observed released-strain range for exploratory xylem analyses.

Surface-released growth strain

Surface-released growth strain (GS) was measured at breast height (1.3 m) in the east, south, west and north directions of each tree. Bark, phloem and cambium were removed to expose a fresh xylem surface. A BE120-10AA-P150 resistance strain gauge was bonded parallel to the grain and connected to a YJW-8 static strain indicator. After zeroing, grooves approximately 5 mm deep were cut above and below the gauge, and the stable released-strain value was recorded [32].

Raw values retained their signs. Reported magnitudes and coefficients of variation used absolute values because the objective was to compare released-strain magnitude and circumferential heterogeneity rather than tensile or compressive sign. A signed-strain sensitivity analysis was also conducted to verify that this transformation did not alter the growth-vigour pattern.

$$\text{Mean absolute GS} = (1/4)\ \Sigma d\ |GSd| \quad \text{(Eq. 1)}$$

$$\text{CVGS (\%)} = SD(|GSd|) / \text{Mean absolute GS} \times 100 \quad \text{(Eq. 2)}$$

where d represents the four cardinal directions.

Disc sampling and axial stem-form descriptors

Discs 2-5 cm thick were cut at 1 m intervals from 0.3 m above ground until the remaining top section was shorter than 3 m. The cylindrical coordinate system used for stem-form measurements is shown in Fig. S2. North was defined as 0°, east as 90°, south as 180° and west as 270°. For each disc, the longest and shortest measured cross-sectional diameters and their azimuths were recorded. These were operational measurements of major and minor diameters; no ellipse fitting, inertia-moment calculation or eigenvector decomposition was applied.

$$\text{Cross-sectional diameter ratio (\%)} = Dmin / Dmax \times 100 \quad \text{(Eq. 3)}$$

$$\text{Radial symmetry ratio (\%)} = R_{short} / R_{long} \times 100 \quad \text{(Eq. 4)}$$

$$\text{Radial-growth CV (\%)} = SD(RGm) / Mean(RGm) \times 100 \quad \text{(Eq. 5)}$$

Here, Dmin and Dmax are the minor and major diameters, Rshort and Rlong are the shorter and longer radii on the major-diameter axis, and RGm is radial growth in direction m.

Major- and minor-diameter azimuths were treated as axial data with 180° periodicity. Their acute included angle was calculated as:

$$\delta = |\alpha_{max} - \alpha_{min}| \bmod 180°; \quad \theta = \min(\delta, 180° - \delta) \quad \text{(Eq. 6)}$$

Thus, θ ranged from 0° to 90° and described the angular relationship between the measured diameter orientations. Diameter-axis reorientation at height h was calculated relative to the 0.3-m reference disc using the shortest 180°-periodic angular difference:

$$\Delta\alpha_h = 0.5 \operatorname{atan2}[\sin 2(\alpha_h - \alpha_{0.3}), \cos 2(\alpha_h - \alpha_{0.3})] \quad \text{(Eq. 7)}$$

Positive and negative values indicate opposite directions of reorientation relative to the reference disc. The measure does not assume continuous clockwise or counter-clockwise twisting. Relative height was calculated as disc height divided by the analysis tree height. Maximum major- and minor-diameter reorientation and the across-height range of the acute included angle were summarised at tree level.

To evaluate how well a single breast-height measurement represented the remainder of the stem, the value at 1.3 m was compared with the mean of all other sampled heights within the same tree. This comparison was made for cross-sectional diameter ratio, radial symmetry ratio, radial-growth CV and acute included angle.

Xylem structural measurements

The six-tree subset was purposively selected to span growth-vigour classes A-D and the observed released-strain range and included two class-A trees, one class-B tree, one class-C tree

and two class-D trees with complete directional strain and xylem data. East, south, west and north samples corresponded to the strain measurement positions. Measurements included microfibril angle (MFA), cellulose crystallinity index (CrI), fibre dimensions, double wall thickness, lumen diameter, wall-lumen ratio and relative FTIR peak-height ratios.

MFA and CrI were determined by X-ray diffraction. MFA was estimated with the 0.6T approach [26] from βT scans between 50° and 150° at a 0.50° step and 10° min^{-1}. CrI profiles were collected over 5-40° 2θ with a 0.020° step and 0.2-s count time at 40 kV and 100 mA. CrI was calculated by the Segal method [20, 27].

$$CrI\ (\%) = [(I002 - Iam) / I002] \times 100 \quad \text{(Eq. 8)}$$

FTIR spectra were collected by the KBr-pellet method over 4000-400 cm^{-1} with 64 scans and 4 cm^{-1} resolution. Each tree-direction sample was measured once. Baseline-corrected, normalised peak-height ratios were interpreted as relative spectral indicators rather than chemical concentrations. Fibre length and width were measured for at least 5000 fibres per tree-direction sample. Double wall thickness and lumen diameter were based on 30 measurements per sample.

Statistical analysis

Tree identity was the biological replicate. Measurements across heights and directions were treated as repeated observations within trees rather than as independent biological replicates. Unless stated otherwise, values are reported as mean ± standard deviation, and $P < 0.05$ was used as the nominal significance level.

Tree-level class comparisons were analysed with linear models containing growth-vigour class and plot as fixed effects. Model residual normality and variance homogeneity were assessed using Shapiro-Wilk and Levene tests, respectively. Type II F tests were used for overall class effects, followed by Tukey HSD comparisons when applicable. Direction-level absolute

184 released growth strain was analysed with a linear mixed-effects model containing direction,
185 growth-vigour class, plot and the direction-by-class interaction as fixed effects and a random
186 intercept for tree. Fixed effects were evaluated by likelihood-ratio tests under maximum
187 likelihood. A GEE analysis with tree as the clustering unit was retained as a sensitivity analysis
188 in Additional file 1.

189 The representativeness of breast-height form was evaluated at the tree level by comparing
190 each 1.3-m value with the mean of the remaining sampled heights. Spearman's rank correlation
191 quantified consistency in tree ranking, whereas Lin's concordance correlation coefficient
192 quantified absolute agreement. Mean signed bias, mean absolute error and the mean within-tree
193 absolute deviation from the breast-height value were also calculated. Spearman P values for the
194 four traits were adjusted by the Benjamini-Hochberg false-discovery-rate procedure.

195 Axial trajectories were analysed with linear mixed-effects models containing plot, growth-
196 vigour class, relative height, relative height squared, and the interactions of class with both
197 height terms as fixed effects. Tree-specific random intercepts and relative-height slopes
198 accounted for repeated discs and individual trajectory differences. Fixed effects were evaluated
199 by likelihood-ratio tests under maximum likelihood, and Benjamini-Hochberg false-discovery-
200 rate correction was applied across the five response traits for each tested effect. For visualisation,
201 fitted curves were restricted to the observed relative-height range of each growth-vigour class.

202 Hierarchical tree-level models tested whether axial form added information about released
203 growth strain beyond tree size and breast-height form. The size block contained plot, DBH and
204 H/D. The breast-height block contained the first two principal-component scores from diameter
205 ratio, radial symmetry ratio, radial-growth CV and acute included angle. The axial block
206 contained the first two principal-component scores from the axial slopes of diameter ratio, radial

symmetry ratio and radial-growth CV, the relative mean-diameter attenuation rate, maximum major-diameter reorientation and the across-height range of the acute included angle. Principal-component loadings and explained variance are reported in Additional file 1.

The increments associated with the breast-height and axial blocks were additionally tested using 9,999 Freedman-Lane residual permutations restricted within plot. Out-of-sample performance was assessed by leave-one-tree-out cross-validation; standardisation, principal-component analysis and model fitting were repeated within each training fold. Predictive performance was summarised by root mean squared error (RMSE) and Q^2. Bootstrap 95% confidence intervals for RMSE and Q^2 were obtained by resampling the 24 held-out observation-prediction pairs 10,000 times.

Single-trait sensitivity analyses paired each breast-height descriptor with its corresponding axial descriptor. These models included plot and growth-vigour class before the breast-height and axial terms were entered sequentially. Standardised regression coefficients and 95% confidence intervals were reported for axial descriptors. Benjamini-Hochberg false-discovery-rate correction was applied across the six single-trait tests.

Primary analyses were conducted in Python 3.12.14 using NumPy 2.5.1, pandas 3.0.3, SciPy 1.18.0 and statsmodels 0.14.6. IBM SPSS Statistics 26.0 was retained for the previously established tree-level and GEE analyses. Figures were prepared using Origin 2021 and Matplotlib 3.11.0.

Use of generative AI-assisted technologies

During manuscript preparation, the authors used OpenAI Codex for English-language refinement, document organisation, and assistance in checking statistical reporting and figure formatting. The authors verified all text, numerical results and figures against the original data

and take full responsibility for the manuscript. No generative AI was used to create or alter experimental data or microscopy images.

Results

The sampling gradient captured differentiation in attained tree size

The 24 sampled trees formed the intended growth-vigour gradient, with six trees per class and equal representation of all classes in both plots. Mean DBH decreased from 21.25 ± 0.68 cm in class A to 14.08 ± 0.77 cm in class D; mean total height declined from 24.18 ± 0.50 to 19.20 ± 1.07 m, while H/D increased (Fig. 1). These contrasts confirmed the Kraft-based sampling gradient used to test the hypotheses; they were not treated as an independent biological result.

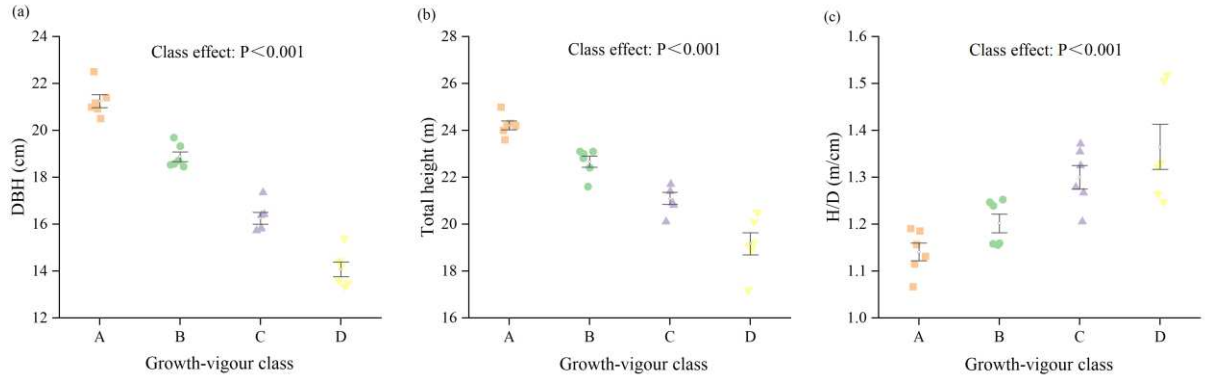


Fig. 1 Tree-size differentiation among growth-vigour classes. Panels show (a) diameter at breast height (DBH), (b) total height and (c) height-to-diameter ratio (H/D). Coloured symbols represent individual trees; open circles and error bars show class means ± standard error. The analysis included 24 trees (n = 6 per class). Overall class effects are shown in each panel; Tukey HSD pairwise results are provided in Additional file 1. These contrasts confirm the intended Kraft-based sampling gradient

Breast-height form did not represent the mean axial state

At breast height, cross-sectional diameter ratio, radial symmetry ratio, radial-growth CV and the acute included angle between the measured major- and minor-diameter orientations

overlapped broadly among growth-vigour classes (Fig. S1). Their breast-height values also showed only weak correspondence with the respective means from the remaining sampled heights (Fig. 2; Table 2).

Absolute agreement was low for all four traits, with Lin's concordance correlation coefficients of 0.025-0.114. Compared with the means at other heights, breast-height values were lower by 4.77 percentage points for diameter ratio, 5.51 percentage points for radial symmetry ratio and 10.47° for included angle, but higher by 2.82 percentage points for radial-growth CV (Table 2). Thus, a breast-height section retained limited ranking information for radial-growth CV and included angle but did not reproduce the average geometric state along the sampled stem.

Table 2. Agreement between breast-height form and the mean of the remaining sampled heights.

Trait	n	Spearman ρ	FDR P	Lin CCC	Bias (BH-other)	MAE	Mean within-tree deviation
Cross-sectional diameter ratio	24	0.251	0.315	0.025	-4.77	4.77	4.64
Radial symmetry ratio	24	0.199	0.351	0.033	-5.51	5.51	5.49
Radial-growth CV	24	0.500	0.026	0.028	2.82	2.82	2.79
Acute included angle	24	0.503	0.026	0.114	-10.47	10.47	10.99

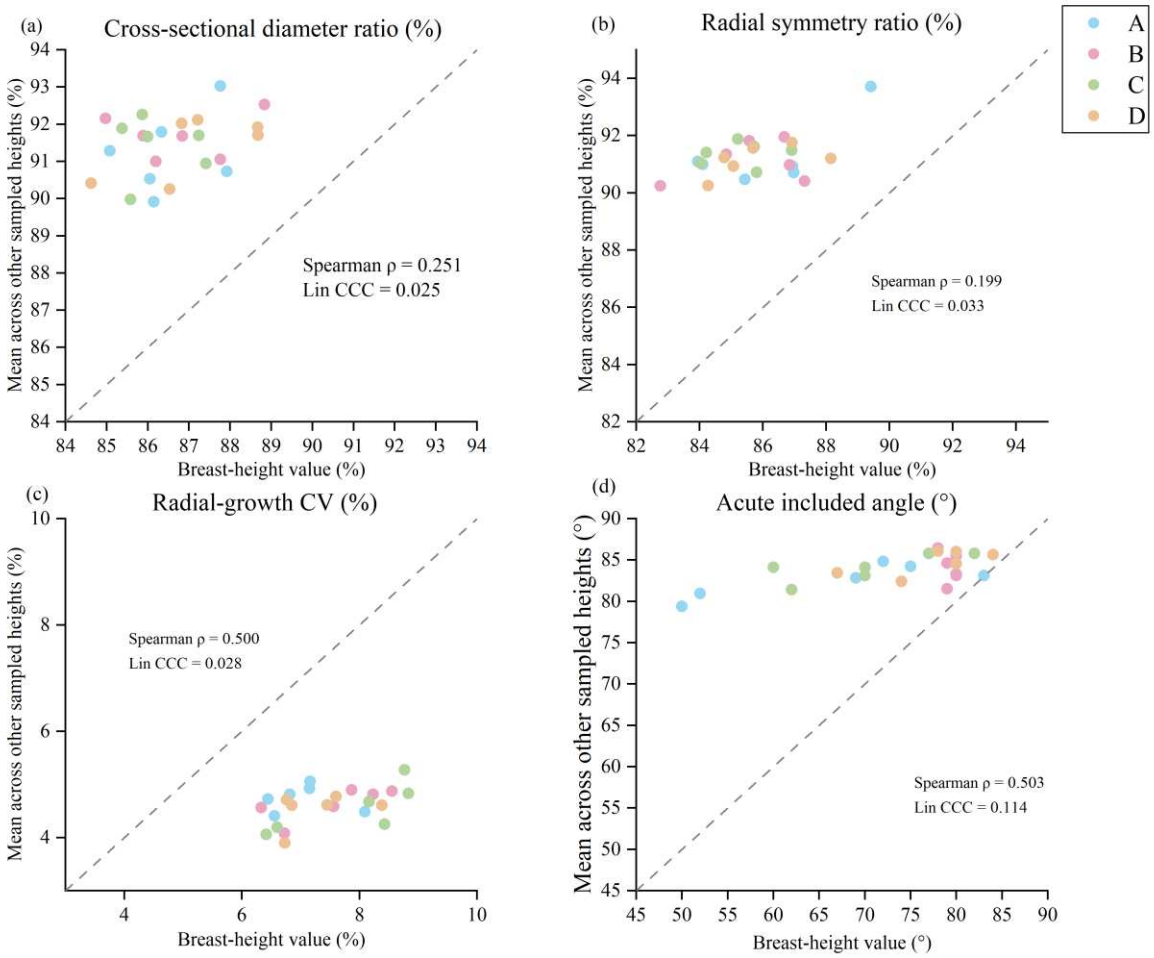


Fig. 2 Representativeness of breast-height form for the remainder of the stem. Breast-height values are compared with the mean across all other sampled heights for (a) cross-sectional diameter ratio, (b) radial symmetry ratio, (c) radial-growth CV and (d) acute included angle between the measured major- and minor-diameter orientations. Each point represents one tree (n = 24); colours and shapes indicate growth-vigour classes. The grey dashed line is the 1:1 line. Spearman's ρ describes rank consistency and Lin's concordance correlation coefficient (CCC) describes absolute agreement

Growth-vigour classes diverged in axial diameter trajectories

Stem geometry changed systematically with relative height. Cross-sectional diameter ratio and radial symmetry ratio generally increased upwards, while radial-growth CV decreased;

major and minor diameters declined over the same interval (Fig. 3). Relative-height effects were detected for all five variables (all $P < 0.001$; Table 3).

Once major and minor diameters were expressed relative to their tree-specific breast-height values, their trajectories differed among growth-vigour classes. Class-by-height effects were retained for relative major diameter (likelihood-ratio $\chi^2(6) = 30.24$, FDR $P < 0.001$) and relative minor diameter ($\chi^2(6) = 29.83$, FDR $P < 0.001$). By contrast, no FDR-significant interaction was detected for diameter ratio (FDR $P = 0.136$), radial symmetry ratio (FDR $P = 0.063$) or radial-growth CV (FDR $P = 0.218$; Table 3). The first hypothesis was therefore supported for normalised diameter trajectories, whereas upward cross-sectional regularisation was broadly shared among classes.

Table 3. Mixed-effects tests of size-adjusted axial stem-form trajectories.

Response	Height LRT $\chi^2(2)$, FDR P	Class LRT $\chi^2(3)$, FDR P	Class × height LRT $\chi^2(6)$, FDR P
Major diameter relative to breast height	176.37, < 0.001	3.63, 0.507	30.24, < 0.001
Minor diameter relative to breast height	180.94, < 0.001	8.46, 0.116	29.83, < 0.001
Cross-sectional diameter ratio	118.72, < 0.001	1.06, 0.894	10.40, 0.136
Radial symmetry ratio	124.72, < 0.001	0.61, 0.894	13.33, 0.063
Radial-growth CV	83.13, < 0.001	7.99, 0.116	8.28, 0.218

Tree-specific random intercepts and relative-height slopes accounted for repeated disc measurements. P values were adjusted within each effect family using the Benjamini-Hochberg false-discovery-rate procedure.

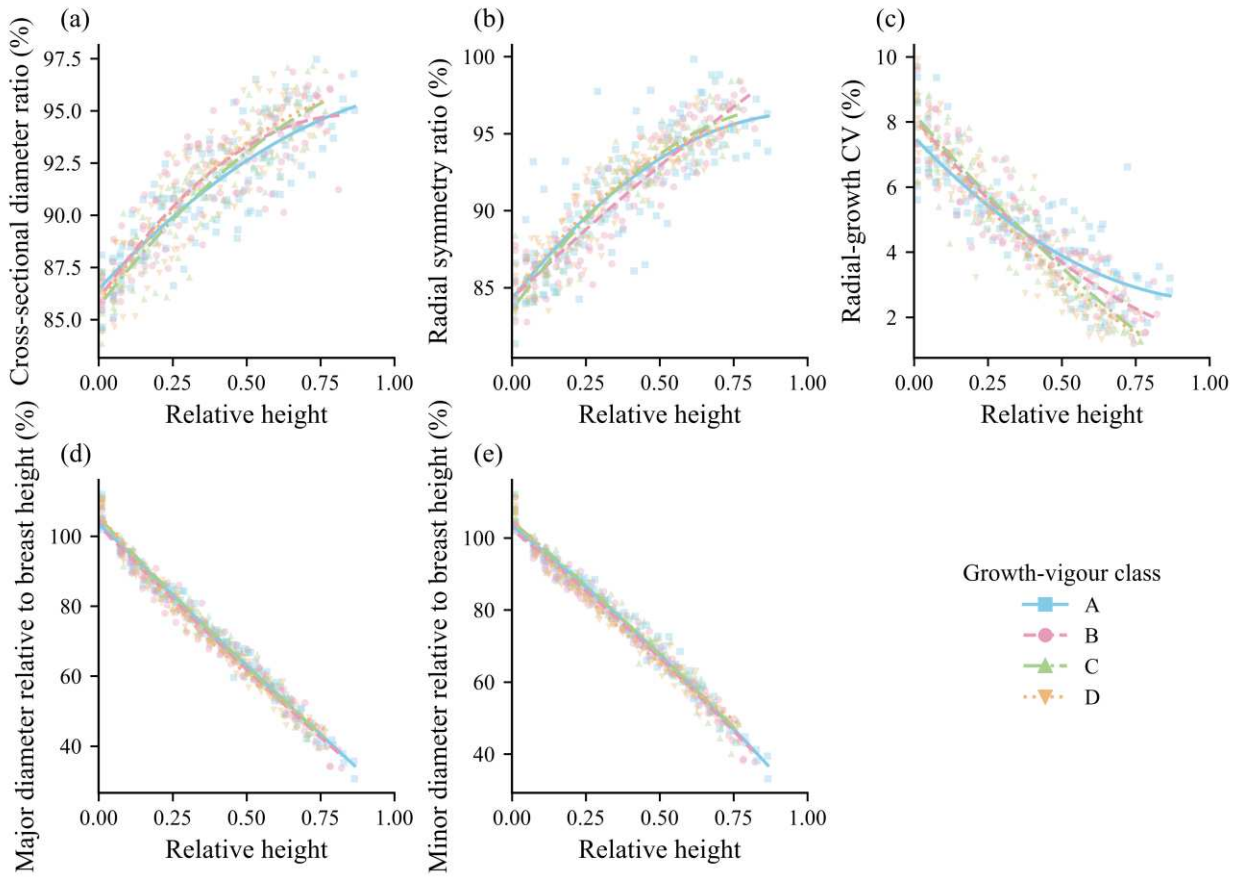


Fig. 3 Axial trajectories of stem geometry along relative height. Panels show (a) cross-sectional diameter ratio, (b) radial symmetry ratio, (c) radial-growth CV, (d) major diameter relative to its breast-height value and (e) minor diameter relative to its breast-height value. Light symbols show repeated disc observations from 24 trees (n = 6 per class); class-specific symbols, line styles and fitted quadratic curves distinguish growth-vigour classes. Each curve is restricted to the observed relative-height range of its class. Mixed-model tests are reported in Table 3

Diameter orientations were reorganised independently along height

Major- and minor-diameter azimuths changed with height relative to the 0.3-m reference disc (Fig. 4). Across trees, maximum major-diameter reorientation ranged from 17° to 82° (median 46°), and maximum minor-diameter reorientation ranged from 33° to 87° (median 57.5°). The acute included angle generally increased towards 90° at greater relative heights. Signed reorientation differed among trees and showed no common clockwise or counter-clockwise sequence.

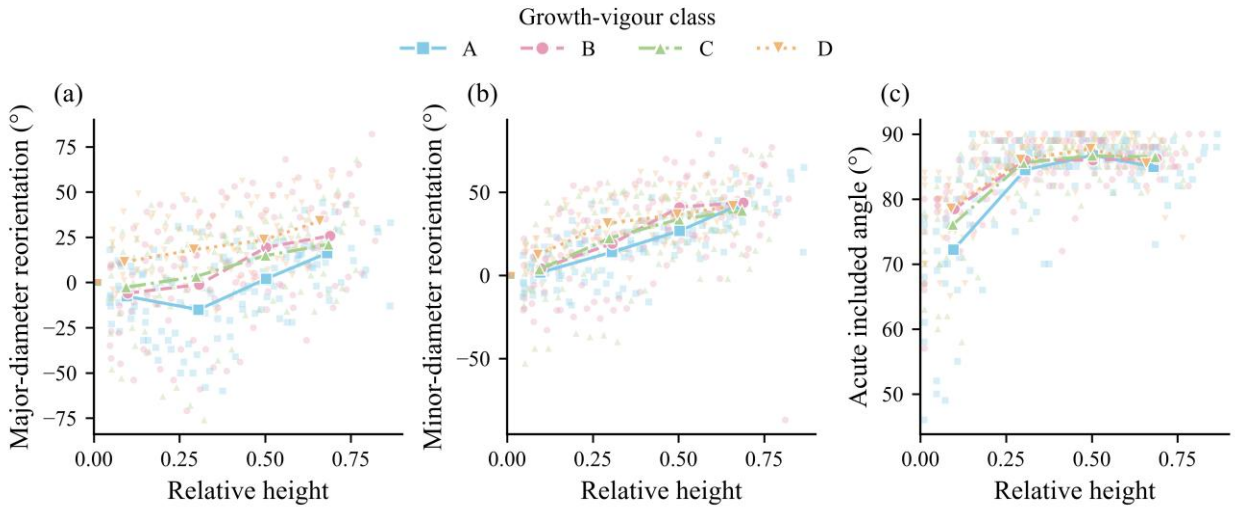


Fig. 4 Diameter-axis reorientation along relative height. Panels show (a) major-diameter reorientation, (b) minor-diameter reorientation and (c) the acute included angle between the measured diameter orientations. Light symbols show repeated disc observations from 24 trees (n = 6 per class). Class-specific symbols and line styles distinguish growth-vigour classes; descriptive segments connect class-wise binned means and are not inferential fits. Reorientation was calculated relative to the 0.3-m reference disc using the shortest 180°-periodic angular difference

Released-strain magnitude and circumferential heterogeneity diverged across vigour classes

Mean absolute released growth strain declined from 854.2 ± 105.4 με in class A to 681.5 ± 111.1 με in class D ($F(3, 19) = 3.49$, $P = 0.036$, partial $\eta^2 = 0.355$; Fig. 5a; Table 4). Circumferential heterogeneity changed in the opposite direction: within-tree SD increased from 139.5 ± 16.5 to 192.9 ± 44.8 με, the range increased from 301.3 ± 36.6 to 428.3 ± 100.7 με, and CV increased from 16.5 ± 2.5% to 28.1 ± 2.8% (Fig. 5b-d). Class effects were detected for SD ($F(3, 19) = 3.34$, $P = 0.041$, partial $\eta^2 = 0.345$), range ($F(3, 19) = 4.41$, $P = 0.016$, partial $\eta^2 = 0.411$) and CV ($F(3, 19) = 10.08$, $P < 0.001$, partial $\eta^2 = 0.614$), supporting the predicted divergence between mean magnitude and circumferential heterogeneity.

Direction-level absolute released growth strain differed among cardinal directions (mixed-model likelihood-ratio $\chi^2(3) = 69.57$, $P < 0.001$) and growth-vigour classes ($\chi^2(3) = 10.53$, $P =$

0.015). The direction-by-class interaction was not significant ($\chi^2(9) = 7.34$, $P = 0.601$), indicating a similar broad directional pattern across classes (Fig. 5e). The GEE sensitivity analysis gave the same qualitative inference (Additional file 1). All 96 raw direction-level values were negative; hence, each tree's signed mean was the exact negative of its mean absolute released growth strain, and the class-model R^2 was unchanged (0.361 in both parameterisations).

Table 4. Tree-level growth-vigour class effects on released growth-strain traits.

Response	**F(3,19)**	**P**	**Partial η^2**
Mean absolute released growth strain	3.49	0.036	0.355
Within-tree SD	3.34	0.041	0.345
Within-tree range	4.41	0.016	0.411
Strain CV	10.08	<0.001	0.614

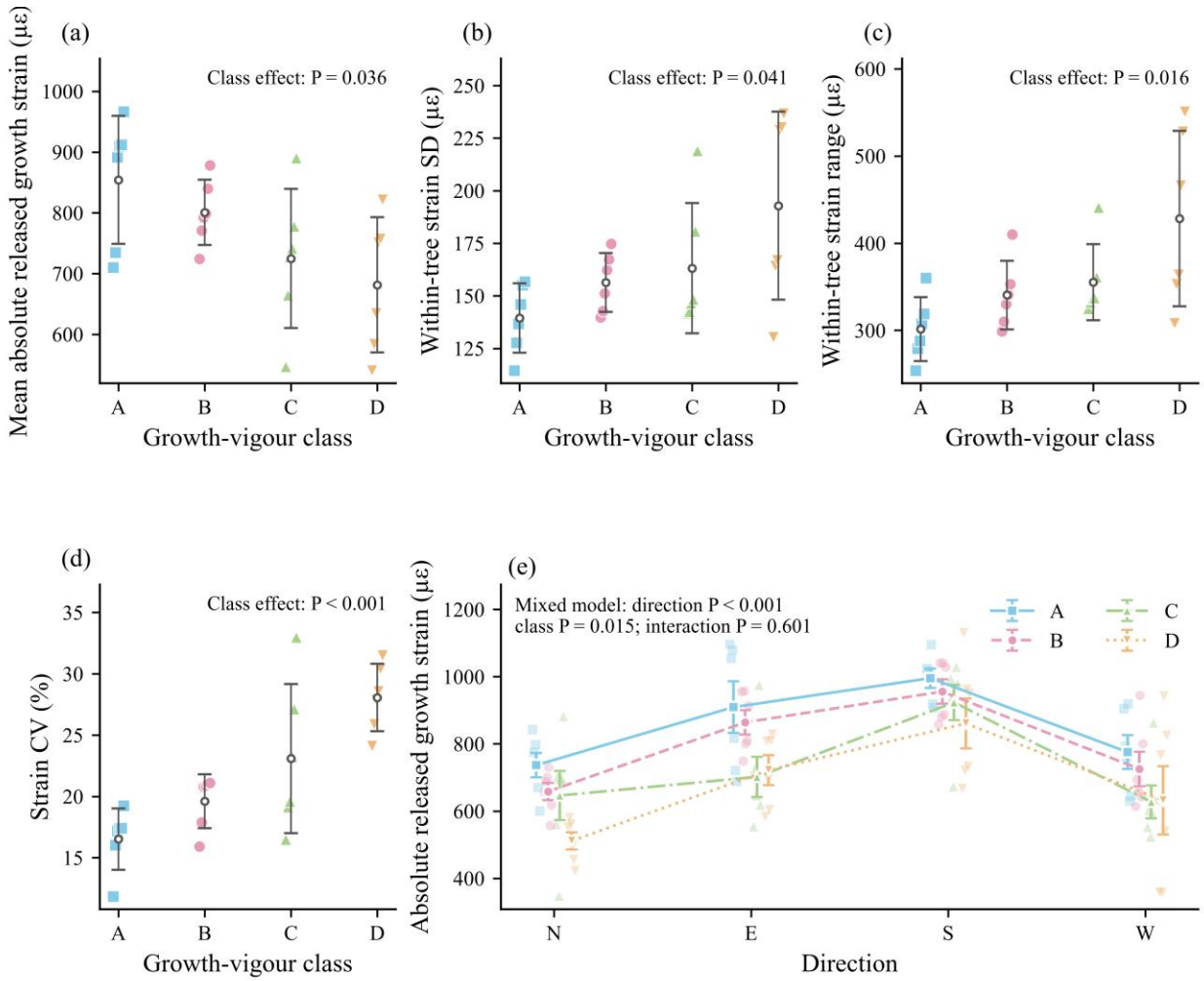


Fig. 5 Released growth-strain magnitude and circumferential heterogeneity among growth-vigour classes. Panels show (a) mean absolute released growth strain, (b) within-tree standard deviation (SD), (c) within-tree range, (d) strain coefficient of variation (CV) and (e) direction-level absolute released growth strain. In panels a-d, class-specific symbols represent 24 individual trees (n = 6 per class), and open circles with error bars show means ± standard error; overall class effects are reported in Table 4. In panel e, light points show four direction-level observations within each tree, and class-specific symbols, line styles and error bars show means ± standard error. Mixed-model direction, class and interaction tests are reported in the text and Additional file 1

Axial form added information about mean released strain

Hierarchical models assessed whether axial descriptors added information about released growth strain beyond tree size and breast-height form (Fig. 6; Table 5). The first two breast-height PCs explained 68.4% of variance in that block, and the first two axial PCs explained

74.4%; their loadings are reported in Additional file 1. For mean absolute released growth strain, adjusted R^2 increased from 0.225 for the size model to 0.585 after adding breast-height form and to 0.890 after adding axial form. The axial increment was supported by restricted permutation ($P < 0.001$). Leave-one-tree-out Q^2 increased from -0.063 to 0.407 and 0.860 across the same sequence. The full model had an RMSE of 42.17 με (bootstrap 95% CI 26.43-56.57) and Q^2 of 0.860 (95% CI 0.721-0.942).

Axial form did not yield comparable gains for circumferential dispersion. For within-tree strain SD, the full model had an adjusted R^2 of 0.111, the axial block was not significant (permutation $P = 0.621$), and leave-one-tree-out Q^2 was -0.328. For strain CV, adjusted R^2 changed from 0.537 after breast-height form was included to 0.528 after axial form was added (permutation $P = 0.362$); Q^2 changed from 0.359 to 0.350. The incremental information in axial form was therefore specific to mean absolute released growth strain rather than SD or CV.

Single-trait sensitivity analyses indicated which axial descriptors contributed to that increment. After the corresponding breast-height trait, growth-vigour class and plot were accounted for, mean absolute released growth strain was negatively associated with the axial slopes of cross-sectional diameter ratio and radial symmetry ratio and positively associated with the axial slope of radial-growth CV and maximum major-diameter reorientation (Fig. 6c; Table 5B). The 95% confidence intervals for these four coefficients excluded zero, whereas those for relative mean-diameter attenuation and included-angle range did not.

Table 5. Hierarchical released-growth-strain models and single-trait axial sensitivity analyses.

(A)

Outcome	Model	Adjusted R^2	AICc	Incremental F, P	Permutation P	LOOCV Q^2
Mean absolute released growth strain	Size	0.225	67.74	-	-	-0.063

Outcome	Model	Adjusted R^2	AICc	Incremental F, P	Permutation P	LOOCV Q^2
Mean absolute released growth strain	Size + BH form	0.585	57.05	9.68, 0.001	<0.001	0.407
Mean absolute released growth strain	Size + BH + axial form	0.890	30.99	25.99, <0.001	<0.001	0.860
Within-tree strain SD	Size	0.241	67.23	-	-	-0.107
Within-tree strain SD	Size + BH form	0.174	73.56	0.19, 0.828	0.816	-0.243
Within-tree strain SD	Size + BH + axial form	0.111	81.14	0.37, 0.697	0.621	-0.328
Strain CV	Size	0.522	56.10	-	-	0.415
Strain CV	Size + BH form	0.537	59.66	1.32, 0.293	0.272	0.359
Strain CV	Size + BH + axial form	0.528	65.96	0.82, 0.456	0.362	0.350

(B)

Axial descriptor	Standardised β	95% CI	Incremental adjusted R^2	FDR P
Cross-sectional diameter-ratio slope	-0.891	-1.088 to -0.695	0.548	<0.001
Radial-symmetry-ratio slope	-0.646	-0.890 to -0.402	0.357	<0.001
Radial-growth-CV slope	0.935	0.560 to 1.310	0.292	<0.001
Included-angle range	0.400	-0.203 to 1.002	0.029	0.216
Maximum major-diameter reorientation	0.553	0.232 to 0.873	0.297	0.003
Relative mean-diameter attenuation	0.133	-0.312 to 0.578	-0.027	0.537

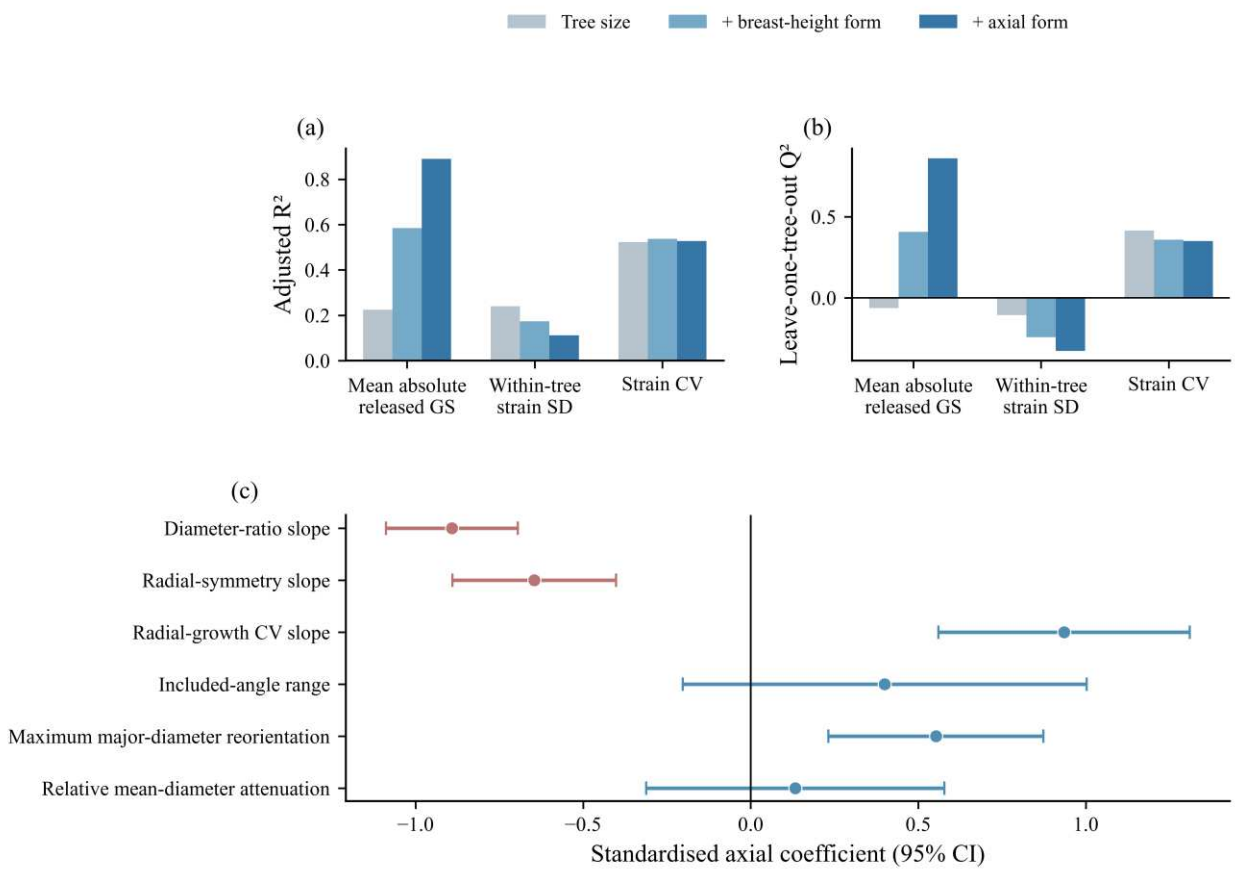


Fig. 6 Incremental information from breast-height and axial stem form in 24 trees. Panels show (a) adjusted R^2 and (b) leave-one-tree-out Q^2 for models containing tree size, tree size plus breast-height form, and the preceding blocks plus axial form; (c) standardised coefficients with 95% confidence intervals for axial descriptors from the single-trait sensitivity models. Positive Q^2 indicates out-of-sample predictive skill. The axial block significantly improved the model for mean absolute released growth strain (restricted permutation $P < 0.001$)

Exploratory xylem traits covaried with the released-strain gradient

The purposively selected six-tree xylem subset spanned growth-vigour classes A-D and the observed range of mean absolute released growth strain. Across these trees, higher strain tended to coincide with lower MFA and higher CrI (Fig. 7). Fibre-wall traits and several relative FTIR peak-height ratios also varied along the strain gradient. These patterns are descriptive and do not estimate population-level association strength.

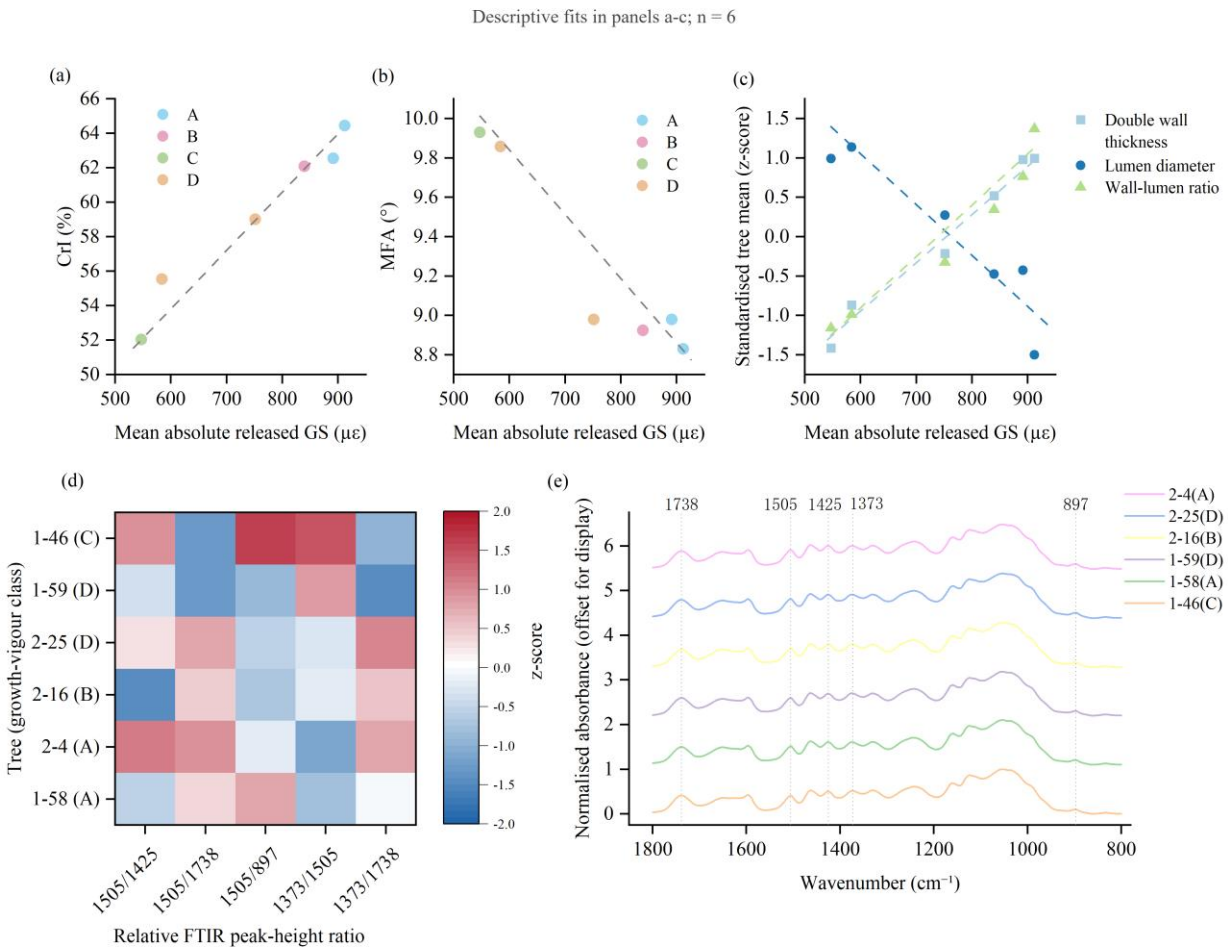


Fig. 7 Exploratory xylem variation along the mean absolute released growth-strain gradient in six purposively selected trees. Panels show the relationships of mean absolute released growth strain with (a) cellulose crystallinity index (CrI), (b) microfibril angle (MFA) and (c) standardised fibre-wall traits; (d) z-scores of relative FTIR peak-height ratios and (e) normalised FTIR spectra. Lines in panels a-c are descriptive fits for n = 6 and are not confirmatory estimates of population-level association strength. Tree labels include growth-vigour class

Discussion

Growth-vigour differentiation extends beyond attained size

H1 was supported for whole-stem diameter trajectories. The four breast-height form traits overlapped broadly among vigour classes and showed little absolute agreement with the corresponding means from the rest of the sampled stem. In contrast, normalised major- and

minor-diameter trajectories differed among classes. Breast-height form and axial organisation therefore captured related but non-interchangeable dimensions of tree development.

This distinction extends the interpretation of growth vigour beyond attained size. Competition contributes to size hierarchy and modifies growth and allometric relationships within stands [6, 11, 12], while growth history can remain embedded in current tree structure [24]. Crown and tree-ring attributes have likewise been combined to evaluate vigour and management needs [10]. In the present *Eucalyptus* stand, repeated discs revealed another component of this structural history: cross sections generally became more regular upwards, but the attenuation of major and minor diameters differed among vigour classes. Axial gradients in wood density, stiffness and microfibril angle have also been reported in *Eucalyptus* [17]. Whole-stem differentiation thus involved the spatial allocation of radial growth, not only differences in final DBH and height.

Growth vigour separates strain magnitude from circumferential heterogeneity

H2 was also supported. Mean absolute released growth strain declined from dominant to suppressed trees, whereas within-tree standard deviation, range and coefficient of variation increased. Average strain magnitude and circumferential heterogeneity therefore represented different components of mechanical state. Dominant trees combined greater mean magnitude with comparatively even circumferential expression, whereas suppressed trees combined lower magnitude with greater directional imbalance.

Released strain in *Eucalyptus* varies with provenance and developmental stage [3, 31], and spatially heterogeneous maturation stress has been documented within plantation stems [8]. Water availability can modify released strain [23], while tree-level growth traits provide additional correlates [18]. The observed class pattern is consistent with growth vigour integrating crown status, resource access and developmental history. Because the study was observational,

however, it cannot distinguish whether social position altered strain development or whether both arose from shared growth conditions.

The absence of a direction-by-class interaction adds an important qualification. Classes differed in overall magnitude and within-tree dispersion, but the broad cardinal-direction pattern was similar. Growth-vigour differentiation therefore affected the level and unevenness of released strain without producing a class-specific circumferential arrangement. This separation also explains why models of mean strain and models of SD or CV responded differently to axial-form information.

Whole-stem organisation adds information about mean released strain

H3 was supported for mean absolute released growth strain. Tree size alone provided limited out-of-sample information. Breast-height form improved model fit and leave-one-tree-out performance, and axial-form components produced a further, larger increment that remained significant under plot-restricted residual permutation. Within the sampled trees, whole-stem organisation was associated with strain variation not represented by DBH, H/D or local cross-sectional form alone. The absence of a comparable increment for strain standard deviation and coefficient of variation shows that this additional information was specific to average strain magnitude.

Single-trait analyses located this additional information in rates of axial change in diameter ratio, radial symmetry ratio and radial-growth CV, together with maximum major-diameter reorientation. Major- and minor-diameter azimuths changed substantially among discs, but their signed changes differed among trees and did not form a common clockwise or counter-clockwise sequence. Reorientation was therefore treated as a shortest 180°-periodic angular difference rather than as continuous bole twisting. Because diameters were measured directly rather than

derived from ellipse fitting, this result concerns measured diameter axes, not formal geometric principal axes. Strain was measured only at breast height, so the model links a local functional measurement to whole-stem structure and does not demonstrate axial variation in strain itself.

Xylem traits provide exploratory structural context

The six-tree subset provided exploratory evidence of structural variation along the released-strain gradient. Higher mean absolute strain tended to coincide with lower microfibril angle and higher cellulose crystallinity, while fibre-wall traits and several relative FTIR peak ratios also varied across the selected trees. Microfibril angle is closely related to longitudinal cell-wall organisation and mechanical behaviour [4, 9]. Cellulose organisation has also been linked to maturation-strain generation [7], and context-dependent control of microfibril orientation is increasingly recognised during reaction-wood formation [30]. These tendencies are compatible with a cell-wall contribution to released-strain expression, but they neither identify the underlying mechanism nor estimate population-level effects.

The FTIR variables likewise represent relative spectral indices rather than direct measurements of lignin, cellulose or hemicellulose content. In addition, the subset comprised only six purposively selected trees spanning the sampled growth-vigour and strain ranges. These results provide exploratory structural context; they cannot estimate population-level correlation strength or establish a complete mechanism.

Biological and silvicultural implications

DBH and total height remain indispensable for plantation inventory, and a breast-height section is appropriate when a local part of the bole is the object of interest. The present results show that growth-vigour classes can also differ in whole-stem organisation and released-strain state. Repeated axial measurements revealed class-dependent diameter trajectories and added

information about mean released strain when local breast-height traits overlapped. This distinction is biologically relevant because trees occupying different social positions can reach different mechanical and structural states through the spatial allocation of growth.

The study did not measure end splitting, sawing distortion or dimensional stability, so the models should not be interpreted as predictions of processing performance. Growth stress is nevertheless a recognised source of processing difficulty [15]. Released stress has been examined through log splitting in *Eucalyptus* [5], and interactions between growth stress and grain can influence splitting among hybrid clones [13]. Forest management increasingly seeks to balance productivity and wood quality [21]. Axial geometry and circumferential strain heterogeneity are therefore suitable candidates for future tests of how stand differentiation translates into usable-wood outcomes.

Limitations and future tests

Inference is limited to 24 trees from two plots within one plantation. Accounting for plot, restricting permutations within plot, correcting for multiple testing and using leave-one-tree-out validation strengthened the within-sample analysis, but these procedures cannot establish causality or population-wide generality. Coefficients from the hierarchical models remain sample-dependent. Replication across plantations, genetic materials, stand densities and environmental conditions is needed to determine whether the observed vigour-form-strain relationships are general.

Released growth strain was measured at breast height, whereas geometry was measured repeatedly along the stem. Future studies should pair strain, geometry and xylem sampling at matched heights and directions. The xylem subset should also be expanded beyond six purposively selected trees before MFA, CrI, fibre-wall traits or relative FTIR indices are used for

class-level inference. Independent plantations and direct measurements of processing outcomes are required to test the practical consequences of the axial descriptors. Within the present limits, the study shows that growth-vigour differentiation encompasses axial stem organisation and distinct components of released-strain state that conventional size measurements do not describe on their own.

Conclusions

Growth-vigour differentiation in this plantation extended beyond attained DBH and height. Breast-height form was a local descriptor and showed little agreement with the mean geometric state of the rest of the sampled stem, whereas repeated measurements revealed class-dependent axial diameter trajectories, upward cross-sectional regularisation and substantial reorientation of measured diameter axes. Dominant trees had greater mean absolute released growth strain but lower circumferential heterogeneity than suppressed trees. Whole-stem axial form added information about mean strain beyond tree size and breast-height form, but did not improve models of strain standard deviation or coefficient of variation. The six-tree xylem subset provided exploratory structural context rather than mechanistic evidence. Together, these results identify whole-stem construction and released-strain heterogeneity as complementary biological dimensions of growth-vigour differentiation in plantation *Eucalyptus*.

Additional files

Additional file 1 (.docx): Supplementary information. Supplementary statistical methods, Figs. S1-S3 and Tables S1-S11, including mixed-model, GEE and signed-strain sensitivity analyses, PCA loadings and explained variance, and LOOCV uncertainty intervals.
Additional file 2 (.xlsx): Corrected tree-level analysis matrix. Tree-level data supporting the agreement and hierarchical analyses.

Additional file 3 (.xlsx): Statistical summary tables. Model outputs and sensitivity analyses.

Additional file 4 (.xlsx): Main-figure source data. Numerical source data for Figs. 1-7.

Declarations

Ethics approval and consent to participate

Not applicable. This study did not involve human participants, human data or animals. Permission to conduct field sampling and collect plant material was granted by Liangfengjiang Forest Farm, the state-owned authority managing the study site.

Consent for publication

Not applicable.

Availability of data and materials

The datasets supporting the conclusions of this article are included within the article and its additional files. The corrected tree-level analysis matrix, statistical summary tables and main-figure source data are provided as Additional files 2-4. Additional raw data and analysis scripts are available from the corresponding author upon reasonable request.

Competing interests

The authors declare that they have no competing interests.

Funding

This work was supported by the Guangxi Natural Science Foundation (No. 2026GXNSFAA00640915) and the Guangxi Forestry Science and Technology Extension Project (Gui Lin Ke Yan [2026KX] No. 30). The funders had no role in the study design, data collection,

analysis, interpretation of data, preparation of the manuscript, or decision to submit the work for publication.

Authors' contributions

YF and PW conceived and designed the study. KX, JH and HZ collected the data. KX analysed and interpreted the data and drafted the manuscript. JH and HZ prepared the visualisations. YF and PW acquired funding, supervised the study and revised the manuscript. All authors read and approved the final manuscript.

Acknowledgements

The authors thank Liangfengjiang Forest Farm for permission to conduct field sampling and collect plant material.

Authors' information

Not applicable.

References

1. Almeras T, Clair B. Critical review on the mechanisms of maturation stress generation in trees. J R Soc Interface. 2016;13:20160550. https://doi.org/10.1098/rsif.2016.0550.
2. Bamber RK. A general theory for the origin of growth stresses in reaction wood: how trees stay upright. IAWA J. 2001;22:205-212. https://doi.org/10.1163/22941932-90000279.
3. Biechele T, Nutto L, Becker G. Growth strain in Eucalyptus nitens at different stages of development. Silva Fenn. 2009;43:669-679. https://doi.org/10.14214/sf.187.
4. Cave ID. Theory of X-ray measurement of microfibril angle in wood. For Prod J. 1966;16:37-42.

5. Chauhan S, Entwistle K. Measurement of surface growth stress in Eucalyptus nitens Maiden by splitting a log along its axis. Holzforschung. 2010;64:267-272. https://doi.org/10.1515/HF.2010.022.

6. Chen B, Liu K, Wang C, Guo J, Lu J, Chen L, Zhao Z, Zeng J. Tree allometry responses to competition and complementarity in mixed-species plantations of Betula alnoides. For Ecosyst. 2024;11:100207. https://doi.org/10.1016/j.fecs.2024.100207.

7. Clair B, Almeras T, Pilate G, Jullien D, Sugiyama J, Riekel C. Maturation stress generation in poplar tension wood studied by synchrotron radiation microdiffraction. Plant Physiol. 2011;155:562-570. https://doi.org/10.1104/pp.110.167270.

8. Clair B, Alteyrac J, Gronvold A, Espejo J, Chanson B, Almeras T. Patterns of longitudinal and tangential maturation stresses in Eucalyptus nitens plantation trees. Ann For Sci. 2013;70:801-811. https://doi.org/10.1007/s13595-013-0318-4.

9. Donaldson L. Microfibril angle: measurement, variation and relationships - a review. IAWA J. 2008;29:345-386. https://doi.org/10.1163/22941932-90000192.

10. Dou X, Zhang X, Kong L, Zhu G, Huang L, Chen G, Liu C, Liu Z. Evaluation and regulation strategies for stand vigour based on crown structure and tree rings of dominant Cunninghamia lanceolata. J For Res. 2026;37:8. https://doi.org/10.1007/s11676-025-01948-2.

11. Ficko A, Beljan K, Vedris M, Cavlovic J, Teslak K. Neighbourhood effects on tree growth in a Fagus sylvatica-Abies alba forest following an ice storm. For Ecosyst. 2024;11:100250. https://doi.org/10.1016/j.fecs.2024.100250.

12. Forrester DI, Bauhus J. A review of processes behind diversity-productivity relationships in forests. Curr For Rep. 2016;2:45-61. https://doi.org/10.1007/s40725-016-0031-2.

13. França FJN, França TSFA, Vidaurre GB. Effect of growth stress and interlocked grain on splitting of seven different hybrid clones of Eucalyptus grandis × Eucalyptus urophylla wood. Holzforschung. 2020;74:917-926. https://doi.org/10.1515/hf-2019-0209.
14. Ghislain B, Clair B. Diversity in the organisation and lignification of tension wood fibre walls - a review. IAWA J. 2017;38:245-265. https://doi.org/10.1163/22941932-20170170.
15. Gril J, Jullien D, Bardet S, Yamamoto H. Tree growth stress and related problems. J Wood Sci. 2017;63:411-432. https://doi.org/10.1007/s10086-017-1639-y.
16. Groover A. Gravitropisms and reaction woods of forest trees: evolution, functions and mechanisms. New Phytol. 2016;211:790-802. https://doi.org/10.1111/nph.13968.
17. Hein PRG, Chaix G, Clair B, Brancheriau L, Gril J. Spatial variation of wood density, stiffness and microfibril angle along Eucalyptus trunks grown under contrasting growth conditions. Trees. 2016;30:871-878. https://doi.org/10.1007/s00468-015-1327-8.
18. Huang Y, Wang J, Pan Y, Zeng H, Fu Y, Wei P. Exploring the relationship between growth strain and growth traits in Eucalyptus cloeziana at different age stages. Sustainability. 2025;17:2229. https://doi.org/10.3390/su17052229.
19. Inoue A, Sato M, Shima H. A new taper index based on form-factor: application to three bamboo species (Phyllostachys spp.). Eur J For Res. 2021;140:1533-1542. https://doi.org/10.1007/s10342-021-01416-6.
20. Li XY, Zhang MH. Relationship of wood moisture content and the degree of crystallinity by X-ray diffraction. J Northeast For Univ. 2014;42(2):96-99.
21. Marziliano PA, Tognetti R, Mercuri M, Labate A, Lombardi F. Balancing stand productivity and wood quality in chestnut coppices using chronosequence approach and productivity model. Eur J For Res. 2022;141:1059-1072. https://doi.org/10.1007/s10342-022-01488-y.

22. Medhurst J, Ottenschlaeger M, Wood M, Harwood C, Beadle C, Valencia JC. Stem eccentricity, crown dry mass distribution, and longitudinal growth strain of plantation-grown Eucalyptus nitens after thinning. Can J For Res. 2011;41:2209-2218. https://doi.org/10.1139/x11-135.
23. Naghizadeh Z, Wessels CB. The effect of water availability on growth strain in Eucalyptus grandis × Eucalyptus urophylla trees. For Ecol Manag. 2021;483:118926. https://doi.org/10.1016/j.foreco.2021.118926.
24. Pretzsch H. Trees grow modulated by the ecological memory of their past growth. For Ecol Manag. 2021;487:118982. https://doi.org/10.1016/j.foreco.2021.118982.
25. Raatevaara A, Korpunen H, Mäkinen H, Uusitalo J. Log end face image and stem tapering indicate maximum bow height on Norway spruce bottom logs. Eur J For Res. 2020;139:1079-1090. https://doi.org/10.1007/s10342-020-01309-0.
26. Ren W, Zhu J, Guo F, Guo J, Wang H, Yu Y. Estimating cellulose microfibril orientation in the cell wall sublayers of bamboo through dimensional analysis of microfibril aggregates. Ind Crops Prod. 2022;179:114677. https://doi.org/10.1016/j.indcrop.2022.114677.
27. Segal L, Creely JJ, Martin AE, Conrad CM. An empirical method for estimating the degree of crystallinity of native cellulose using the X-ray diffractometer. Text Res J. 1959;29:786-794. https://doi.org/10.1177/004051755902901003.
28. Schmucker J, Uhl E, Steckel M, Pretzsch H. Crown allometry and growing space requirements of four rare domestic tree species compared to oak and beech: implications for adaptive forest management. Eur J For Res. 2022;141:587-604. https://doi.org/10.1007/s10342-022-01460-w.

29. Thibaut B, Gril J. Tree growth forces and wood properties. Peer Community J. 2021;1. https://doi.org/10.24072/pcjournal.48.

30. Tobias LM, McFarlane HE, Bossinger G, Spokevicius AV. Cortical microtubule dynamics during reaction wood formation ensures context-appropriate cellulose microfibril angle in woody trees. Trees. 2024;38:507-522. https://doi.org/10.1007/s00468-024-02497-7.

31. Yang JL, Fife D, Matheson AC. Growth strain in three provenances of plantation-grown Eucalyptus globulus Labill. Aust For. 2001;64:248-256. https://doi.org/10.1080/00049158.2001.10676196.

32. Yoshida M, Okuyama T. Techniques for measuring growth stress on the xylem surface using strain and dial gauges. Holzforschung. 2002;56:461-467. https://doi.org/10.1515/HF.2002.071.

Supplementary Files

This is a list of supplementary files associated with this preprint. Click to download.

- Additionalfile1.docx